# Chapter 7

# A Direct Study of Grain Boundary Allotriomorphic Ferrite Crystallography

## 7.1 Introduction

The work presented in the previous chapters has emphasised a beneficial role of thin layers of allotriomorphic ferrite layers on removing the austenite grain surfaces as potential nucleation sites for bainite, and hence forcing a microstructural transition from bainite to acicular ferrite when suitable intragranular nucleation sites are available in sufficient numbers (Fig. 4.13c). This beneficial effect of allotriomorphic ferrite has to be balanced against its undesirable ability to stimulate the formation of Widmanstätten ferrite or bainite.

When Widmanstätten ferrite grows from allotriomorphic ferrite, it is contiguous with the latter. Thus, allotriomorphic ferrite can only develop into Widmanstätten ferrite if it has the "right" orientation relationship with the austenite, since Widmanstätten ferrite is a product of displacive transformation. This orientation lies within the so-called "Bain region", within which no plane or direction is rotated by more than about 11° from the Bain orientation (Crosky *et al.*, 1980). The classical Kurdjumov-Sachs (KS) and Nishiyama-Wasserman (NW) orientation relationships lie within this region. The crystallography of allotriomorphic ferrite is therefore of crucial importance in determining whether its presence will have the desired effect of facilitating intragranular nucleation of acicular ferrite, or the undesirable effect of providing a substrate for the nucleation of Widmanstätten ferrite. It is almost certain that grain boundary allotriomorphic ferrite, when it nucleates, has a good fitting orientation relationship (within the Bain region) with one of the austenite grains with which it is in contact. The ferrite grows, however, by reconstructive transformation. The rate of growth would be faster at incoherent interfaces, *i.e.*, in those austenite grains with which the ferrite is "randomly" orientated. The growth process could thus lead to a situation in which the majority of allotriomorphic ferrite/austenite interface is incoherent and hence incapable of developing into Widmanstätten ferrite.

The purpose of the present work was to determine the fraction of ferrite allotriomorphs which, as a consequence of the wrong crystallography generated by selective growth, are unlikely to lead to Widmanstätten ferrite formation. Similar crystallographic experiments have been reported previously (King and Bell, 1975), but the austenite orientation was deduced indirectly by assuming specific habit plane indices for Widmanstätten ferrite plates, indices which are now known to be different (Watson and McDougall, 1973). Experiments have been designed here which allow the retention of large quantities of austenite permitting the direct measurement of its orientation.

## 7.2 Experimental Methods

### *7.2.1 Alloys and Heat Treatment*

The chemical compositions (wt.%) of the two Fe–C–Si–Mn alloys studied are given in Table 7.1. The steels were prepared as 20 kg vacuum induction melts from high purity base materials. The ingots were forged and hot rolled to 10 mm diameter rods, followed by swaging to 3 mm diameter rods. They were then homogenised at 1200 °C for 3 days while sealed in quartz capsules containing pure argon.

In low alloy steel, usually on cooling to room temperature, there will be very small amounts of retained austenite. The aim of the present work has been to study the crystallography of allotriomorphic ferrite directly with austenite. Hence, the steel studied is of wrought alloy and different composition from the alloy used in previous chapter. The relatively high silicon concentration of the alloys ensures that carbides do not precipitate during the formation of upper bainite (Bhadeshia and Edmonds, 1979). Consequently, the carbon that is partitioned into the residual austenite stabilises it to further transformation, with substantial quantities of austenite being retained to ambient temperature. This austenite is of value in directly assessing the crystallography of any transformation products. Two–stage step heat treatments were designed to take advantage of this characteristic, to obtain mixed microstructures of allotriomorphic ferrite, bainitic ferrite and retained austenite. After austenitisation, the samples were partially isothermally transformed to a small volume fraction of allotriomorphic ferrite at a temperature $T_1$, followed by a second isothermal heat treatment at a lower temperature $T_2$ in order to induce the formation of upper bainitic ferrite. The amount of allotriomorphic ferrite was kept small in order to study the early stages of the reaction, before impingement between different allotriomorphs can confuse interpretation. Consequently, it is the subsequent growth of bainitic ferrite which leads to a larger extent of carbon enrichment in the residual austenite, necessary to prevent much of the untransformed austenite at $T_2$ from decomposing martensitically during the final quench to ambient temperature. The treatment at $T_1$ was in some cases omitted in order to study the crystallography of bainite in its own right.

### *7.2.2 Metallography*

Thin foil samples for transmission electron microscopy were prepared using the procedure outlined in chapter 2. The samples were examined in *Philips* EM300 and EM400T transmission electron microscopes operated at 100 and 120 kV respectively.

Figure 7.1a shows the optical micrograph of allotriomorphic ferrite along the austenite grain boundaries and Fig. 7.1b shows typical bainitic sheaves observed within the austenite grain grains. Microanalysis experiments were carried out on the EM400T, using an energy

Table 7.1 Chemical composition (wt.%) and details of the heat treatments. The austenitisation conditions were 1000 °Cand for 5 minutes.

| Alloy | C | Si | Mn | $T_1$ °C/Time | $T_2$ °C/Time |
|---|---|---|---|---|---|
| A1 | 0.40 | 2.03 | 3.00 | 703/10 h | 340/12 h |
| A2 | 0.22 | 2.03 | 3.00 | 640/ 1 h | 340/140 min |

dispersive X-ray analysis facility. The specimens, which were about 100 nm thick, were held in a beryllium holder tilted 35° from the normal. The X-ray count rate was optimised at about 1000 counts $s^{-1}$, over a count period of 100 s. The data were analysed using the *LINK RTS 2 FLS* program for thin foil microanalysis; this corrects the data for atomic number and absorption effects and accounts for overlapping peaks by fitting standard profiles. Even though the probe diameter was about 2-5 nm, beam spreading due to the scattering of electrons within the thin foil gave an estimated broadened beam diameter of about 20 nm, a size which was small enough for the purposes of the investigation.

### 7.3 Crystallographic Technique

Austenite/ferrite orientations outside the Bain region generally arise during reconstructive transformation in which growth is not restricted by austenite grain boundaries, so that a particle can grow into regions which had little or no influence in determining its orientation during the nucleation stage. Although the ferrite may nucleate from austenite with an orientation within the Bain region, it can then grow with a random orientation into adjacent austenite grains. The probability of finding ferrite which is well related to the adjacent austenite depends therefore on the growth stage; the aim here is to detect whether or not the orientation of ferrite which has grown well beyond the nucleation stage has an orientation within the Bain region, since only then is it capable of nucleating secondary Widmanstätten ferrite plates. To distinguish the Bain region from random orientations does not require extreme precision of the kind associated with Kikuchi line measurements. The experimental data presented here are based on an analysis of the reciprocal lattice vectors observed in conventional selected area electron diffraction patterns. The zone axis of each pattern can then deviate typically by 5° from the optic axis of the microscope, and this can be used as an estimate of the error. In fact, the error should be somewhat smaller since the orientations were deduced not from the zone axes, but by examining the relationship between pairs of reciprocal lattice vectors (in the same diffraction pattern) from each of the two crystals concerned. The four reciprocal lattice vectors

were then used to determine the coordinate transformation matrix defining the orientation relationship, in the manner described elsewhere (Yang and Bhadeshia, 1989a and Bhadeshia, 1987b).

The validity of the method was checked by measuring the orientation relationship between bainitic ferrite and its parent austenite; the displacive transformation mechanism ensures that the orientation should always lie well within the Bain region, with a pair of corresponding close–packed planes and a pair of corresponding close–packed directions within those planes being approximately parallel. Data from 16 sets of measurements are summarised in Fig. 7.2, where the angle between the close–packed planes $\{111\}_\gamma$ and $\{011\}_\alpha$ is designated $\theta$, and that between the directions $< 10\bar{1} >_\gamma$ and $< 11\bar{1} >_\alpha$ is designated $\phi$. The data are, as expected, all within the Bain region. The mean value of the angle $\theta$ was found to be 2.5° with a standard deviation of 1.9° whereas the corresponding mean and standard deviation for $\phi$ were 3.4 and 2.0° respectively. Given that $\theta$ is expected to be very close to zero (within about 0.5°), the analysis confirms that the error associated with the technique is small enough to distinguish between random and Bain–region orientations.

## 7.4 Results and Discussion

### *7.4.1 Allotriomorphic Ferrite/Austenite Orientation Relations*

Figure 7.3 revealed that the two–stage heat treatment resulted in the desired microstructure, consisting of small allotriomorphs of ferrite at the austenite grain boundaries, and sheaves of bainitic ferrite and retained austenite. Facets which appeared to be growth ledges were observed on the allotriomorphic ferrite indicated by the arrow in Fig. 7.3, on the side of the allotriomorph which had a near KS relation with the austenite. An other remarkable example of the crystallographic data obtained using transmission electron microscopy and electron diffraction is presented in Fig. 7.4 which will be discussed in detail after a presentation of all the crystallographic data. Occasionally, the allotriomorphic ferrite in alloy A1 seemed to contain manganese rich, unidentified carbides as seen in Fig. 7.5 and Table 7.2.

The complete set of crystallographic data are presented in Tables 7.3 & 7.4, for alloys A1 and A2 respectively. In these tables, an "a" appearing after the identification number represents the orientation relationship between the allotriomorph and the adjacent austenite grain $\gamma_1$, whereas "b" denotes the orientation of the same allotriomorph with respect to the other austenite grain ($\gamma_2$) with which it is in contact. We also adopt the convention here that the $\alpha/\gamma_1$ orientation is chosen to be the one that is better with respect to lattice matching than the $\alpha/\gamma_2$ orientation. In one particular case, where the ferrite was found at a three–grain junction, a letter 'c' was used to identify its orientation with the third austenite grain. The orientation

Table 7.2. Microanalysis data on allotriomorphic ferrite, bainite and carbide on alloy A1 & A2 after step heat treatment. The compositions of the austenite and ferrite in equilibrium were calculated using the National Physical Laboratory MTDATA system (1989). Note the absence of partitioning for bainitic ferrite, confirming the microanalysis technique.

| Allotriomorphic ferrite | | | |
|---|---|---|---|
| Element | Observed | Equilibrium | Alloy |
| Mn | 1.6 | 1.00 | A1 (703 °C) |
| Si | 2.5 | 2.68 | A1 (703 °C) |
| Mn | 1.8 | 1.16 | A2 (640 °C) |
| Si | 1.9 | 2.40 | A2 (640 °C) |
| **Bainitic ferrite** | | | |
| Element | Observed | Expected | Alloy |
| Mn | 3.1 | 3.00 | A1 |
| Si | 2.0 | 2.03 | A1 |
| Mn | 3.2 | 3.00 | A2 |
| Si | 2.3 | 2.03 | A2 |
| **Carbide** | | | |
| Element | Observed | Expected | Alloy |
| Mn | 12.6 | - | A1 |
| Si | 0.4 | - | A1 |

data are summarised for convenience in terms of the angles $\theta$ and $\phi$ defined earlier, although the full coordinate transformation matrix which completely defines the $\alpha/\gamma$ orientation relation was available for each case. They results are also illustrated graphically in Fig. 7.6.

Out of a total of 19 cases examined in detail each case consisting of an allotriomorphic ferrite and its adjacent $\gamma$ grains, only 7 were consistent with an $\alpha/\gamma_1$ orientation relation within the Bain region, the majority of the orientation relationships being more or less random. The seven cases were found to be consistent with the C. S. Smith (1948) hypothesis in that the ferrite in each case revealed a tendency to crystallographically facet on the side with the Bain region related austenite, whereas curved boundaries were apparent on the other side with which it was randomly orientated. In only one case was the ferrite orientation such as to be within the Bain region with respect to both of the adjacent austenite grains within the limits of experimental error (Case 15, Table 7.3).

Only a small fraction of allotriomorphs are therefore found to be in the right crystallographic orientation to provide a substrate for secondary Widmanstätten ferrite growth (the fact that Widmanstätten ferrite did not form is because the alloys were heat-treated above the Widmanstätten ferrite start temperature). It is very likely that this result cannot be attributed to the orientation relationships that develop during nucleation. In order to avoid a large activation barrier, the ferrite must nucleate with a good match with at least one of the austenite grains with which it is in contact (Aaronson and Russel, 1981). Nucleation would therefore demand that all allotriomorphs should exhibit orientations within the Bain region. However, the original orientation distribution will be changed if the allotriomorphs grow into regions far from their original nucleation sites. This can happen if growth occurs at a higher rate along those austenite grains boundaries with which the ferrite has high energy (*i.e.*, high mobility) interfaces. Purdy (1978), using hot-stage transmission electron microscopy, has directly demonstrated the higher mobility of interfaces between ferrite and austenite which are randomly orientated. The smaller extent of ferrite penetration into the Bain region related austenite (Fig. 7.4), compared with growth into the other randomly orientated austenite grain is consistent with Purdy's work.

The orientation data (Tables 7.3 & 7.4) are consistent with the earlier studies of Ryder and Pitsch (1966) and King and Bell (1975). Although the present work reveals a rather smaller fraction of allotriomorphs with an orientation within the Bain region, any quantitative comparisons are doubtful since the crystallographic textures of the materials used are unlikely to be identical. The texture must influence the relative orientations of the austenite grains and hence the crystallography of the ferrite that forms subsequently. This may also explain why King and Bell found a larger fraction of allotriomorphs with a good match with both the adjacent austenite grains.

### *7.4.2 Ferrite Orientation with Respect to Both Adjacent Austenite Grains*

It is only by coincidence that a ferrite grain nucleates with a reproducible orientation relationship with both of the austenite grains with which it is in contact. In general, it is only expected to have an orientation relationship with one of the parent austenite grains. It nevertheless seems reasonable that the ferrite should attempt to choose a variant of this orientation relation which allows the highest degree of matching with the other austenite grain, even though its orientation with the second grain may not be ideal.

The seven cases for which the ferrite was found to have an orientation within the Bain region (Tables 7.3 & 7.4) were analysed further to study whether the ferrite makes any attempt during nucleation to optimise lattice matching with both the austenite grains. For the other data, the crystallography suggests that the allotriomorphs have grown away from their original

Table 7.3. Summary of $\alpha - \gamma$ orientation relationship in alloy A1.

| Number | $\theta$ | $\phi$ | Approx. Orientation |
|---|---|---|---|
| 1a | 4.04 | 3.2 | KS/NW |
| 1b | 27.6 | 22.0 | - |
| 2a | 0.0 | 5.0 | NW |
| 2b | 18.1 | 32.1 | - |
| 3a | 15.1 | 4.9 | - |
| 3b | 13.7 | 13.6 | - |
| 4a | 0.0 | 5.3 | NW |
| 4b | 19.9 | 15.8 | - |
| 4c | 35.3 | 33.5 | - |
| 5a | 2.0 | 5.5 | KS/NW |
| 5b | 20.5 | 16.4 | - |
| 6a | 15.0 | 16.8 | - |
| 6b | 18.9 | 22.5 | - |
| 7a | 8.7 | 10.7 | - |
| 7b | 24.5 | 10.1 | - |
| 8a | 5.7 | 23.5 | - |
| 8b | 28.9 | 28.5 | - |
| 9a | 0.0 | 19.8 | - |
| 9b | 24.3 | 10.6 | - |
| 10a | 18.7 | 11.3 | - |
| 10b | 26.4 | 26.4 | - |
| 11a | 14.4 | 17.0 | - |
| 11b | 25.5 | 23.8 | - |
| 12a | 28.5 | 21.4 | - |
| 12b | 21.4 | 30.8 | - |
| 13a | 30.3 | 24.4 | - |
| 13b | 24.4 | 26.8 | - |
| 14a | 0.0 | 8.9 | - |
| 14b | 2.7 | 28.7 | - |
| 15a | 3.0 | 5.8 | KS/NW |
| 15b | 6.9 | 5.3 | $\simeq$ KS/NW |

Table 7.4 Summary of $\alpha - \gamma$ orientation relationships for alloy A2.

| Number | $\theta$ | $\phi$ | Approx. Orientation |
|---|---|---|---|
| 1a | 0.9 | 21.0 | |
| 1b | 20.1 | 20.1 | |
| 2a | 14.2 | 13.0 | |
| 2b | 25.7 | 17.0 | |
| 3a | 3.9 | 6.2 | KS/NW |
| 3b | 27.3 | 26.2 | |
| 4a | 3.8 | 5.6 | KS/NW |
| 4b | 23.6 | 31.5 | |

sites, the observed orientations no longer being representative of the nucleation stage.

The degree of $\alpha/\gamma_2$ fit was assessed by calculating the determinant of the matrix $T$, which represents the ratio of the volume of the unit cell of the Bollmann's O-lattice to that of volume of the unit cell of the reference crystal. The O-lattice is a set of points of perfect fit between the two crystal lattices which are allowed notionally to interpenetrate and fill all space. Hence, the smaller the value of the determinant, the better is the fit between the two crystals. The matrix $T$ can be deduced from a knowledge of the deformation $S$ which converts the lattice of one of the crystals into that of the other (the *reference* lattice). The deformation $S$ can be deduced from a knowledge of the coordinate transformation matrix $J$ (representing the orientation relationship) and an assumed correspondence matrix $C$. $J$ is of course, measured experimentally whereas $C$ is taken to be the Bain correspondence; the magnitude of the deformation $S$ depends on the specific variant of the Bain correspondence, which in each case is chosen to be that which leads to the smallest determinant of $T$. Details of these methods can be found in reference (Christian, 1975).

Considering a $\gamma_1/\alpha/\gamma_2$ tricrystal, in which the $\gamma_1/\alpha$ orientation is within the Bain region, the symmetry of cubic crystals suggests that there are in general, twenty four variants of $(\alpha\ J\ \gamma_1)$.† Of these twenty four possibilities, one corresponds to the experimentally measured orientation, and the task here is to discover whether this particular variant of the orientation relationship also gives the best match with the crystal $\gamma_2$, *i.e.*, the one which gives the smallest value of the determinant of $(\gamma_2\ T\ \gamma_2)$, where

† The notation used here is due to Bowles and Mackenzie (1954), and suggests that $J$ is a $3 \times 3$ coordinate transformation matrix describing the orientation relationship between $\alpha$ and $\gamma_1$. Each column of $J$ represents the components of a basis vector of $\gamma_1$ in the basis $\alpha$.

$$(\gamma_2\ T\ \gamma_2) = I - (\gamma_2\ C\ \alpha)(\alpha\ J\ \gamma_2). \tag{7.1}$$

In none of the seven cases examined did the allotriomorph seem to attempt to lattice match with both of the adjacent austenite grains. Thus, the experimental variant of the $(\alpha\ J\ \gamma_1)$ orientation did not correspond to the smallest possible value of the determinant of $(\gamma_2\ T\ \gamma_2)$, as illustrated in Fig. 7.7. The ratio of calculated minimum determinant value for $(\gamma_2\ T\ \gamma_2)$ for a given variant and the actual determinant value observed for $(\gamma_2\ T\ \gamma_2)$ is presented in Fig. 7.8, which summarises the variant analysis. The result is difficult to explain, but could indicate that the orientation of the austenite grain boundary plane might have an effect on the choice of the orientation variant (Aaronson and Russel, 1981).

*7.4.3 Bainite/Austenite Grain Boundary Crystallography*

The opportunity was taken during the allotriomorphic ferrite experiments, to measure also the orientations of grain boundary nucleated bainite and the adjacent austenite grains (Table 7.5). Similar to the results obtained for allotriomorphic ferrite, the bainite did not seem to choose an orientation variant with its parent austenite which gave the optimum matching with the other austenite grain.

Table 7.5: Alloy A1. Summary of bainite orientation relationship with the austenite grain in which it is growing (a), and with the grain on the other side of the boundary (b).

| Number | $\theta$ | $\phi$ | Approx. Orientation |
|---|---|---|---|
| 1a | 0.0 | 5.3 | NW |
| 1b | 10.5 | 10.3 | - |
| 2a | 0.0 | 0.5 | KS |
| 2b | 11.4 | 0.0 | - |
| 3a | 0.7 | 0.0 | KS |
| 3b | 3.3 | 0.0 | KS/NW |
| 4a | 4.3 | 6.4 | KS/NW |
| 4b | 0.7 | 5.3 | NW |
| 5a | 0.06 | 0.0 | KS |
| 5b | 14.9 | 0.0 | - |
| 6a | 0.0 | 0.06 | KS |
| 6b | 15.0 | 0.0 | - |

*7.4.4 Detailed Examination of a Particular Allotriomorph*

One of the experiments (Case 1, Table 7.3) revealed an exceptionally good example of an allotriomorph which exhibited microstructural features consistent with its $\alpha/\gamma_1$ orientation being well within the Bain region, and a random $\alpha/\gamma_2$ orientation (Fig. 7.4). With the $\gamma_1$ grain, the ferrite exhibited a very pronounced tendency to crystallographically facet, giving a clearly ledged transformation interface. Whether these ledges are growth ledges, or simply facetting which results from tendency of the particle to minimise interfacial energy, can only be decided by observing the growth. Their non-uniform height and spacing (Fig. 7.9) is consistent with theory for ledged growth (Atkinson, 1982), but such variations can also be expected from facetting. The important point is that the facets represent planes of low interfacial energy around the particle.

The crystallographic indices of the facet planes were measured using a method of trace analysis which avoids ambiguity. Because the interface planes were inclined to the foil surface, their projected widths within the foil and contrast conditions can be used to measure their inclinations, which can in turn be used to fix the interface plane uniquely; the fringe contrast also helps to fix the sense of inclination of the interface plane. The results are plotted on Fig. 7.10, which also illustrates the interfacial energy minima calculated by Ecob and Ralph (1981). It is evident from Fig. 7.10, that within the limits of experimental error, the present data are approximately consistent with those calculations.

A further interesting feature is that the $\alpha/\gamma_1$ side of the boundary has been able to nucleate a plate of bainite (Fig. 7.4 & 7.11) during the second stage of the heat-treatment (below the bainite-start temperature). This is consistent with the discussion earlier that only allotriomorphs whose orientation lies within the Bain region can be active in nucleating the products of displacive transformation (*e.g.* bainite, Widmanstätten ferrite). By contrast, a transformation-free region is observed on the other side ($\alpha/\gamma_2$) where the allotriomorph is randomly orientated. It is also interesting to note that the trace of the bainite habit plane for the plate nucleated from the allotriomorph does not coincide with the facet planes on the allotriomorph (Fig. 7.11). The bainite habit plane should be determined by the minimisation of strain energy due to the shape change accompanying transformation, rather than interfacial energy minimisation.

*7.4.5 Chemical Composition of Allotriomorphic Ferrite*

It is of interest to examine the chemical composition of the allotriomorphic ferrite formed in the two alloys because the alloys A1 and A2 had respectively been heat-treated at temperatures above and below the paraequilibrium Ae3' curve of the phase diagram (Fig. 7.12). Paraequilibrium is a condition of constrained equilibrium in which the iron to substitutional solute atom ratio is constant everywhere during transformation, but subject to that constraint,

the carbon attains the same chemical potential in all phases. Thus, the Ae3' curve defines the composition of the austenite which is in paraequilibrium with ferrite. The curves presented in Fig. 7.12, and the thermodynamic calculations presented in Table 7.2, were calculated as in references (MTDATA, 1989 and Bhadeshia and Edmonds, 1980). The experimental data presented in Table 7.2 represent the bulk chemical compositions of the ferrite allotriomorphs, and conclusively demonstrate that both the manganese and silicon partition during the growth of ferrite in both the alloys, for the transformation conditions described earlier. Furthermore, although partitioning is found, its extent is less than that expected from equilibrium considerations (Table 7.2) and the growth process is best described as *nonequilibrium.*

For the transformation conditions used, it is thermodynamically impossible for the ferrite in alloy A1 to grow by a paraequilibrium mechanism, so that the partitioning of manganese and silicon is necessary during transformation. Since alloy A2 was transformed below the Ae3' phase boundary (Fig. 7.12), it is *thermodynamically* possible for the ferrite to form with paraequilibrium; this does not however, rule out growth with local equilibrium at the interface, or indeed with any of an infinite set of conditions between equilibrium and paraequilibrium. The exact mode of transformation must be decided by kinetic considerations. A method for estimating the transition from equilibrium to paraequilibrium involves the calculation of the extent $z$ of the diffusion field of the solute element (Coates, 1973a):

$$z \simeq 2D/v \tag{7.2}$$

where $D$ is the diffusivity of the solute concerned in the parent phase, and $v$ is the interfacial velocity, which for the present circumstances is time dependent ($v = \alpha_1 t^{-0.5}$, where $\alpha_1$ is the one–dimensional parabolic thickening rate constant and $t$ is the growth time). Coates suggested that if $z$ is found to be less than about 1 nm, then growth could be assumed to occur by a paraequilibrium mode, since the diffusion distance is then negligible.

The velocity was estimated by measuring the mean allotriomorph half–thickness ($q$) and dividing by the isothermal transformation time. This might lead to an underestimation of $v$ since an incubation period may be necessary before the nucleation of ferrite, an approximation which would lead to an overestimation of $z$. The values of $z$ were found to be $z_{Mn} \simeq 18\,\text{nm}$ and $z_{Si} \simeq 4\,\text{nm}$ for alloy A1 in which the transformation was carried out at the higher temperature (above Ae3'). For alloy A2, on the other hand, both of the calculated diffusion distances were found to be incredibly small at $z_{Mn} \simeq 8 \times 10^{-2}\,\text{nm}$ and $z_{Si} \simeq 0.14\,\text{nm}$. In contradiction to the experimental evidence for alloy A2, this suggests that allotriomorphic ferrite growth should occur by a paraequilibrium mechanism.

As first pointed out by Coates, the diffusion distance criterion for assessing the onset of

paraequilibrium growth is unlikely to be correct, since conventional diffusion theory breaks down as the concentration gradients become large. Hillert (1981) has also pointed out that the criterion fails to predict the experimental observations on pearlite and massive ferrite.

Aziz (1982) has developed a model for solute trapping during rapid solidification, which is likely to be a better representation of nonequilibrium growth (Olson *et al.*, 1990). If the actual ratio (partition coefficient) of the solute concentration in the product to that in the parent phase at the interface is written $k_p$, and the equilibrium ratio $k_e$, he finds that

$$k_p = (1 + \beta k_e)/(1 + \beta) \tag{7.3}$$

where $\beta = D/(v\lambda)$, $\lambda$ being the intersite diffusion distance assumed to be 0.25 nm. As $k_p$ tends towards unity, growth tends towards paraequilibrium. For the present experiments, assuming that the measured ferrite concentration can be used to estimate $k_p$,† the theory is found to predict correctly that substitutional solute partitioning should occur during the growth of ferrite in alloy A2. The partition coefficients were calculated to be $k_p^{Mn} \simeq 0.7$ and $k_p^{Si} \simeq 1.7$.

### 7.5 Summary & Conclusions

By using a steel containing a large silicon concentration, and a two–stage heat treatment procedure, it has been possible to produce a microstructure consisting of allotriomorphic ferrite, bainitic ferrite and retained austenite. This permitted a direct examination of the crystallography of grain boundary allotriomorphs of ferrite. It is found that the fraction of allotriomorphs which have an orientation (with the parent austenite) which is in the Bain region is rather small. This has implications on the theory for the prediction of microstructure in steel welds, where a thin layer of allotriomorphic ferrite is required to promote the intragranular formation of acicular ferrite, as long as it can be prevented from nucleating Widmanstätten ferrite at the same time. This qualitative conclusion has to be backed by further research before the fraction of active allotriomorphs can be predicted. Such work must consider the role of crystallographic texture in the parent austenite, and of its subsequent rate of transformation to allotriomorphic ferrite.

Most of the allotriomorphs do not seem to attempt to maximise lattice matching with both of the grains with which they are in contact, and it is speculated that this might be due to an influence of austenite grain boundary orientation in determining variant selection.

It has been shown that the transition to paraequlibrium growth as the transformation temperature is reduced, cannot be predicted by estimating the extent of the solute diffusion

† It is really the concentrations at the transformation interface which are of relevance, so that the calculated values of $k_p$ cannot be compared directly with our experimental data, although they can certainly be used to indicate whether growth should involve a substantial degree of partitioning.

field in the austenite during allotriomorphic ferrite growth. A possible way forward would be to utilise solute trapping theory, in a manner applied already to coupled diffusional/displacive transformations (Olson *et al.*, 1990), to predict the partitioning coefficient as a function of undercooling below the equilibrium transformation temperature.

---

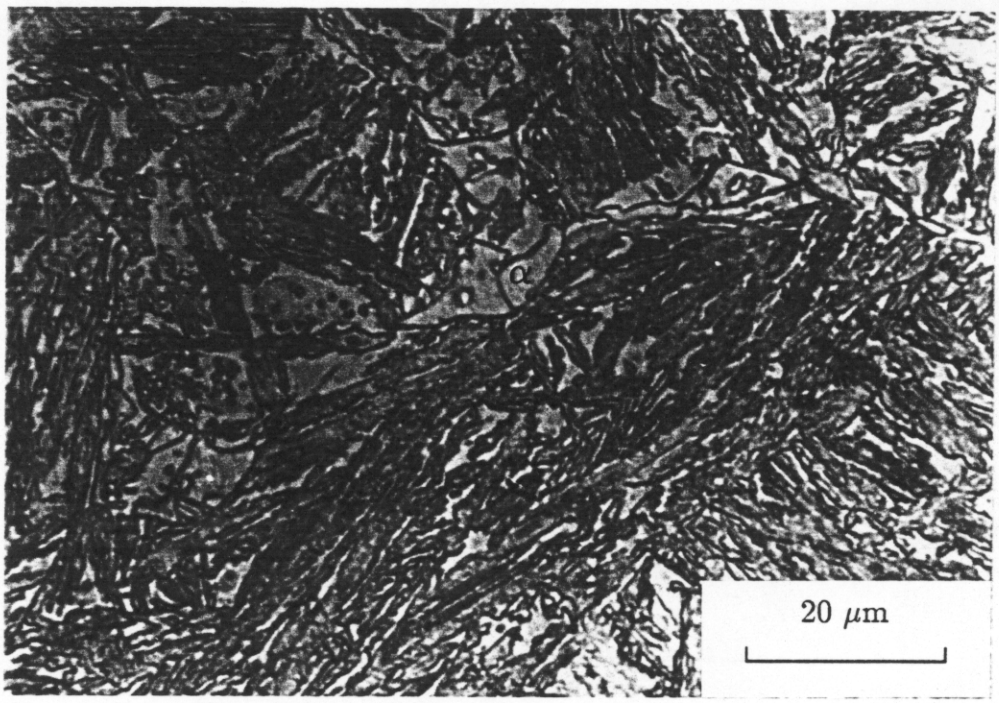


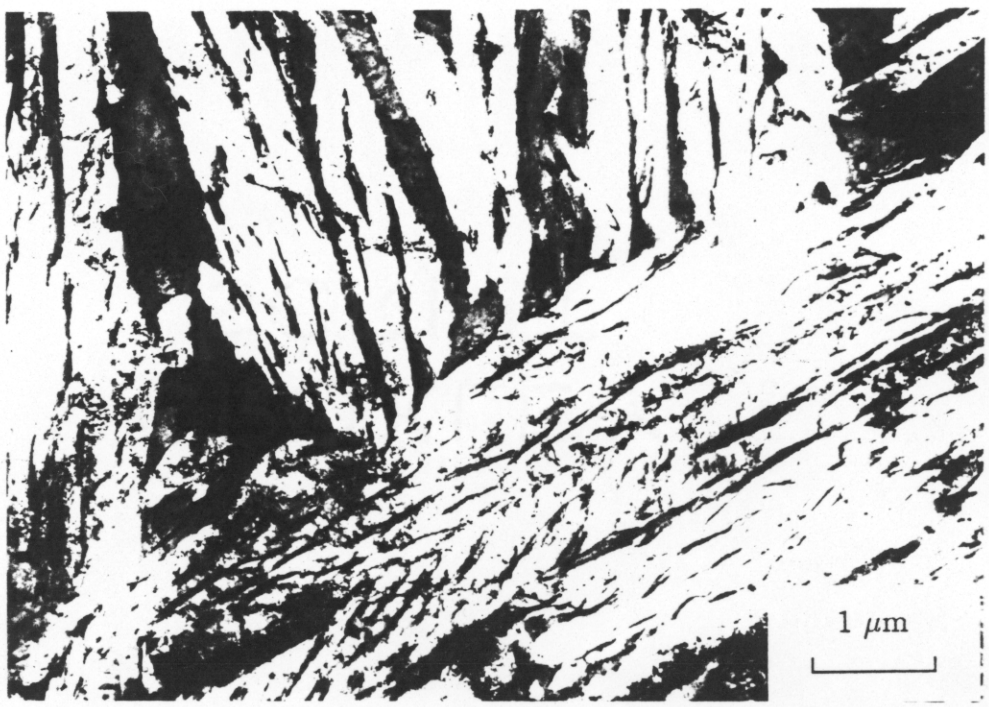


Fig. 7.1 Microstructure observed in alloy A1 after the step heat treatment as mentioned in Table 7.1

a. Optical micrograph of alloy A1, indicating the allotriomorphic ferrite all along the austenite grain boundaries.

b. Transmission electron micrograph of A1, illustrating the sheaf structure of bainite.

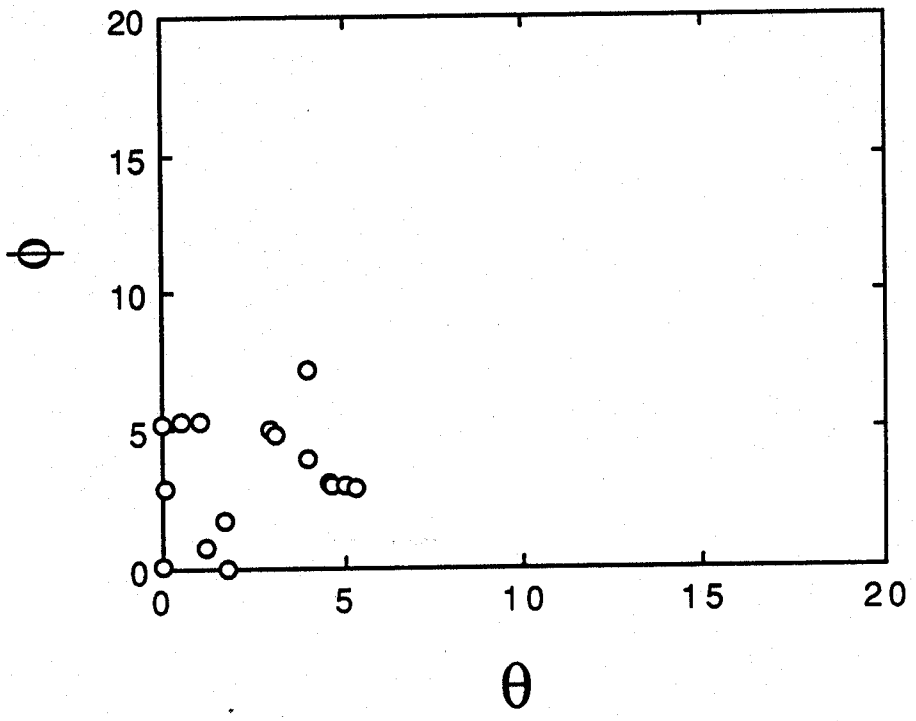


Fig. 7.2 Graphical presentation of summary of $\alpha - \gamma$ orientation relationship for 16 cases of bainite, where $\theta$ is the angle between $\{ 1\,1\,1 \}_\gamma - \{ 0\,1\,1 \}_\alpha$ and $\phi$ is the angle between $< 1\,0\,\bar{1} >_\gamma - < 1\,1\,\bar{1} >_\alpha$.

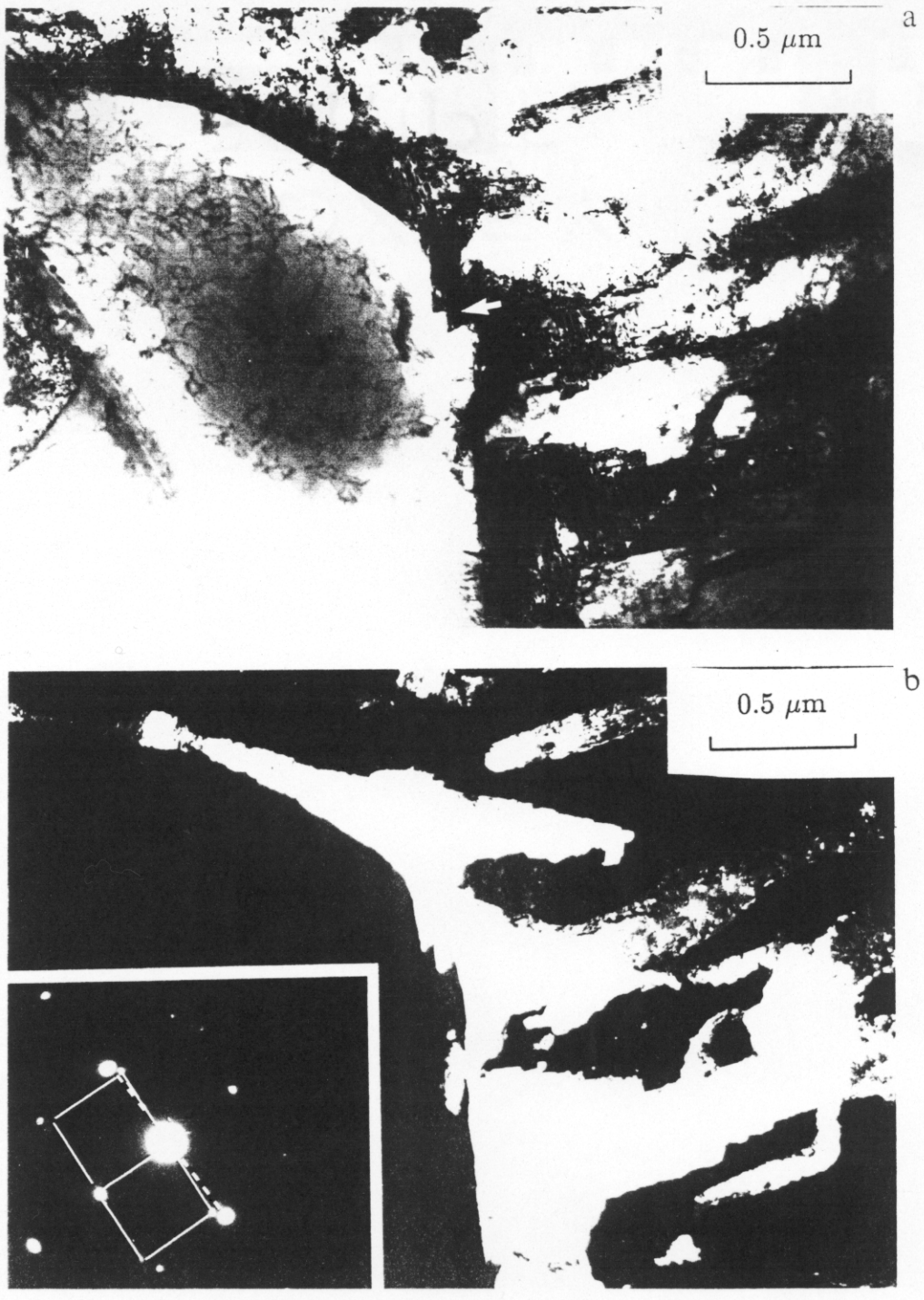


Fig. 7.3 Microstructure obtained in alloy A1 after the step heat treatment. (a) Bright field micrograph illustrating allotriomorphic ferrite, bainite and retained austenite, (b) corresponding dark field micrograph for the residual austenite. The inset is the diffraction pattern from the allotriomorphic ferrite and austenite (solid line is ferrite < 001 > zone axis and dotted line is austenite).

Fig. 7.4 (a) Bright field electron micrograph exhibiting an allotriomorphic ferrite nucleated from austenite grain boundary (marked as B), and bainitic sheaves growing from austenite grain boundary and also within the grain. (b) Diffraction pattern from the allotriomorphic ferrite and $\gamma_1$ a near KS/NW orientation relation, (c) the diffraction pattern of austenite $\gamma_2$ from the random orientation side of allotriomorphic ferrite, consisting of other reflections due to bainitic ferrite also. The $\gamma_2$ reflections are used for finding orientation relation ($\alpha J \gamma_2$), by overlapping the two diffraction patterns appropriately (see overleaf).


B
1 μm
(a)

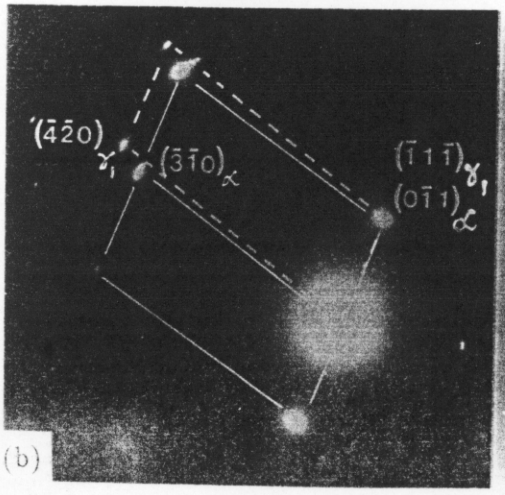
(4̄2̄0)γ
(3̄1̄0)α
(1̄1 1̄)γ
(0 1̄ 1)α
(b)

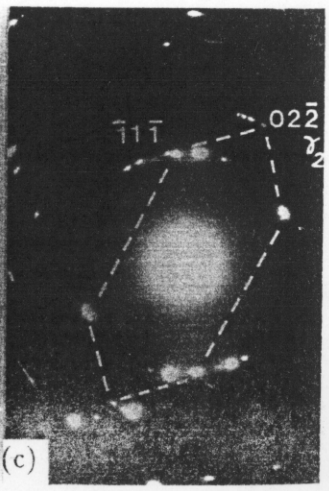
1̄1 1̄
02 2̄
γ
(c)

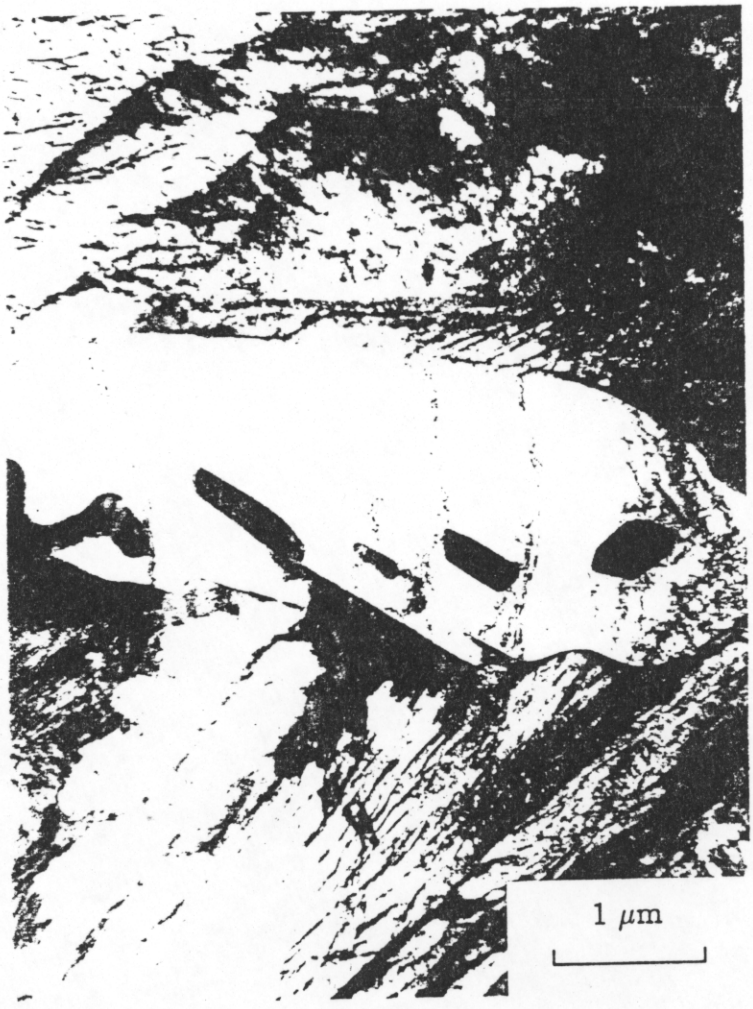


Fig. 7.5 An allotriomorphic ferrite in alloy A1 with carbides. The morphology suggest that the precipitation might have occurred during transformation to ferrite, explaining the apparent coverage by single allotriomorphic grain.

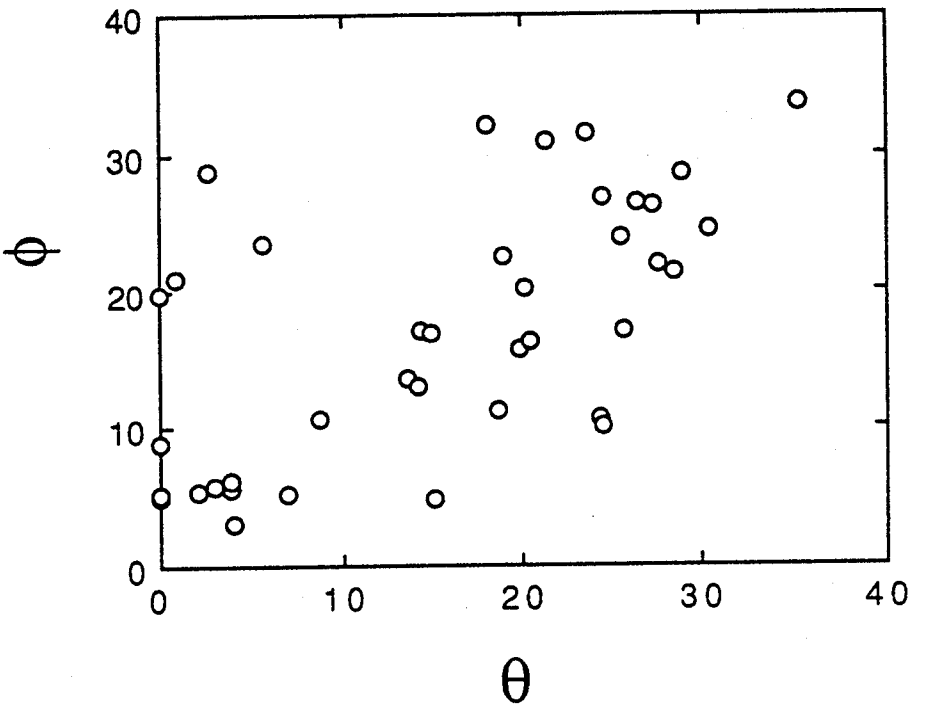


Fig. 7.6 Graphical presentation of summary of $\alpha - \gamma$ orientation relationship, data from Table 7.3 & 7.4, where $\theta$ is the angle between $\{ 1\ 1\ 1 \}_\gamma - \{ 0\ 1\ 1 \}_\alpha$ and $\phi$ is the angle between $< 1\ 0\ \bar{1} >_\gamma - < 1\ 1\ \bar{1} >_\alpha$.

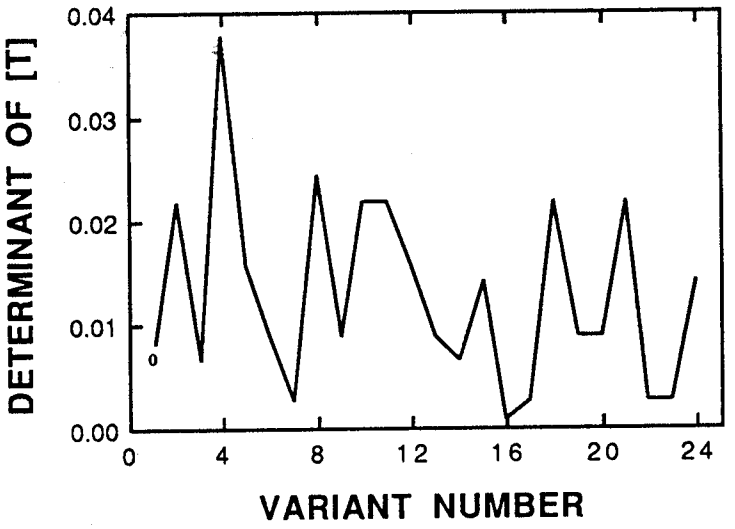


Fig. 7.7 Plot of variation of determinant value of $T$ matrix, as discussed in the text. The point (for variant 1) indicates the determinant of $T$ matrix obtained using the experimentally observed orientation relationship, $(\alpha J \gamma_2)$.

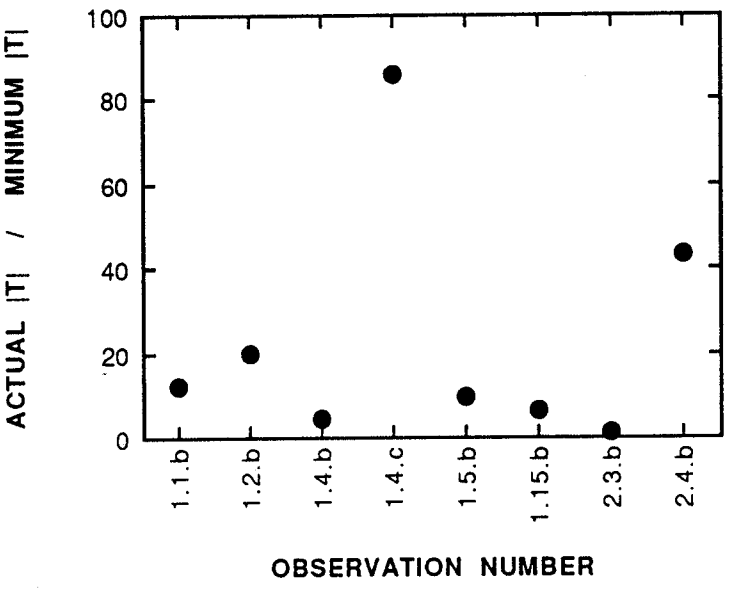


Fig. 7.8 Summary of variant analysis on allotriomorphic ferrites which exhibited near KS/NW with one of the austenite grain. The ratio of determinant value of observed $(\gamma_2 T \gamma_2)$ to that of calculated minimum determinant value is plotted for all the cases. Prefix 1 & 2 correspond to the data from alloy A1 and A2, respectively (Tables 7.3 & 7.4); ideally a value of 1 is expected to indicate a good fitting with $\gamma_2$ for a given $(\alpha J \gamma_1)$ variant.

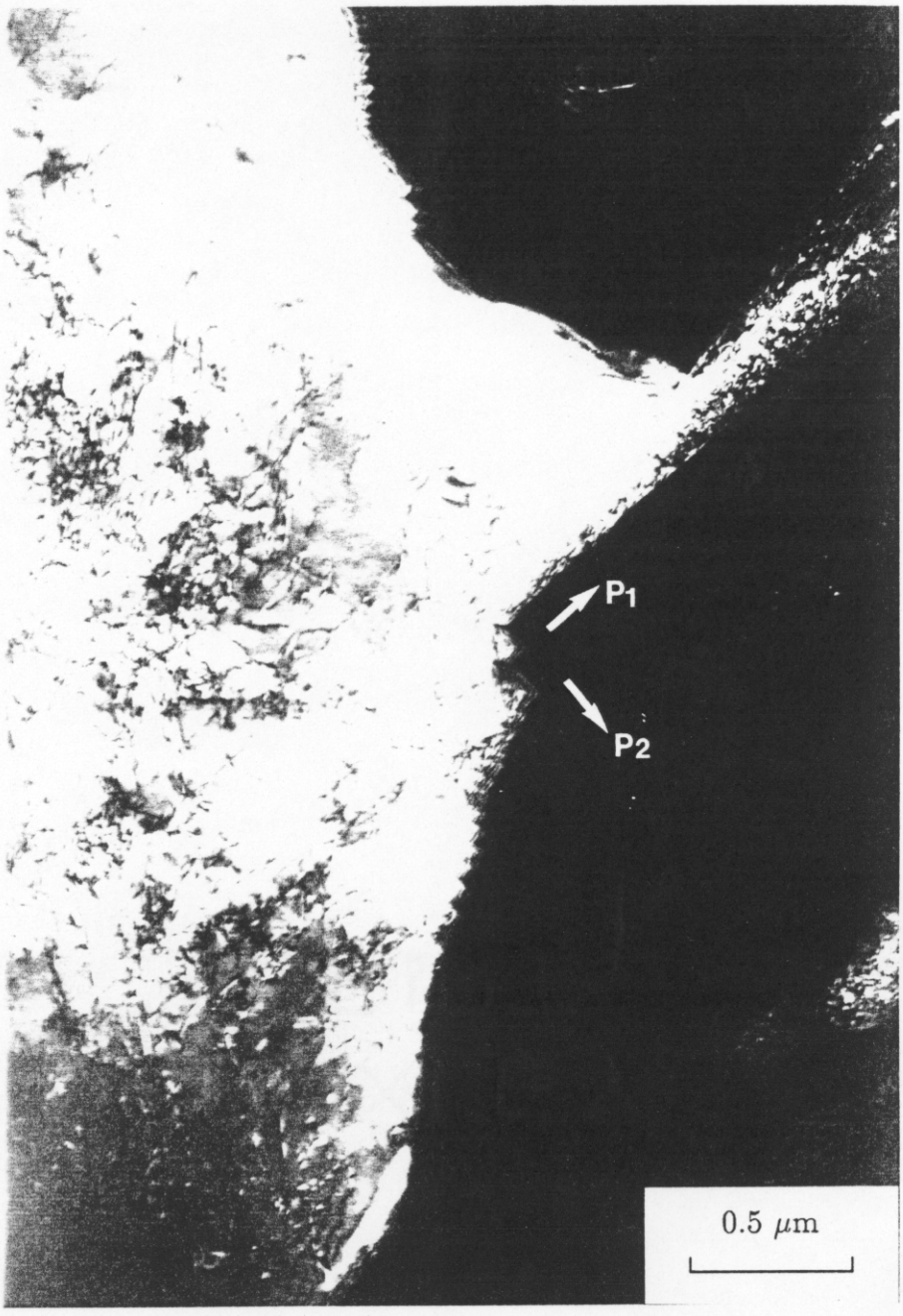


Fig. 7.9 The micrograph of the interface which showed KS/NW relation with the austenite, exhibiting ledge type faceted interface. The ledge height can be seen to vary over the width of the ferrite, apparently increasing towards the nucleation site of bainite.

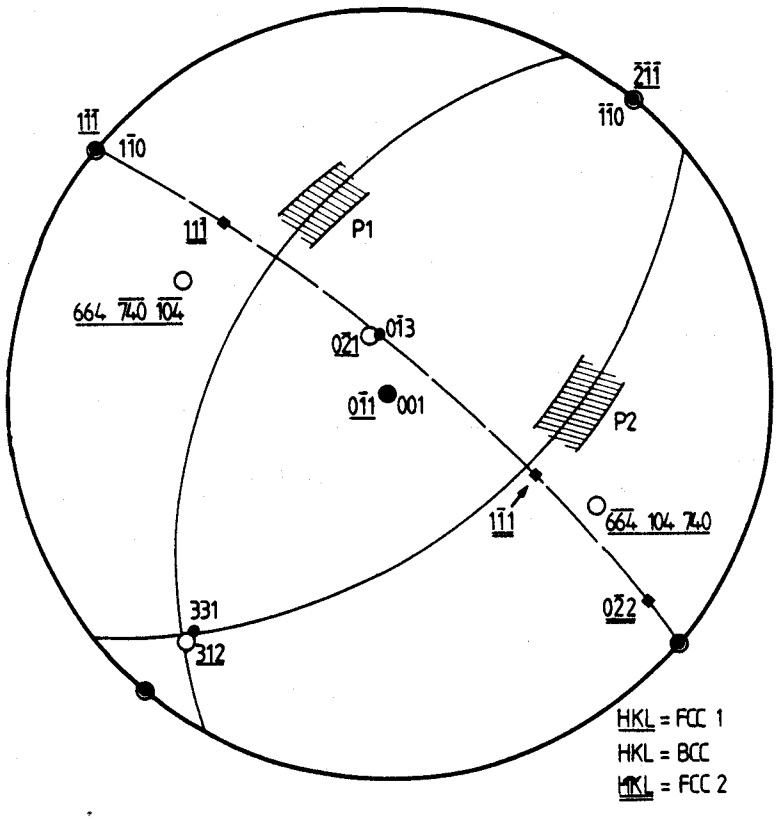


Fig. 7.10 Stereogram plot of interface plane calculations for the allotriomorphic ferrite interface which exhibited KS/NW (case 1 of Table 7.3), and exhibited ledge type interface. The stereogram is overlap of $[\ 0\ 0\ 1\ ]_{\alpha}$ and $[\ 0\ \bar{1}\ 1\ ]_{\gamma}$ zone axes. The low energy equilibrium interface planes calculated by Ecob and Ralph (1981) are also plotted.


Fig. 7.11 Enlarged image of Fig. 7.4, indicating the region where bainitic ferrite appears to grow directly from the allotriomorphic ferrite.

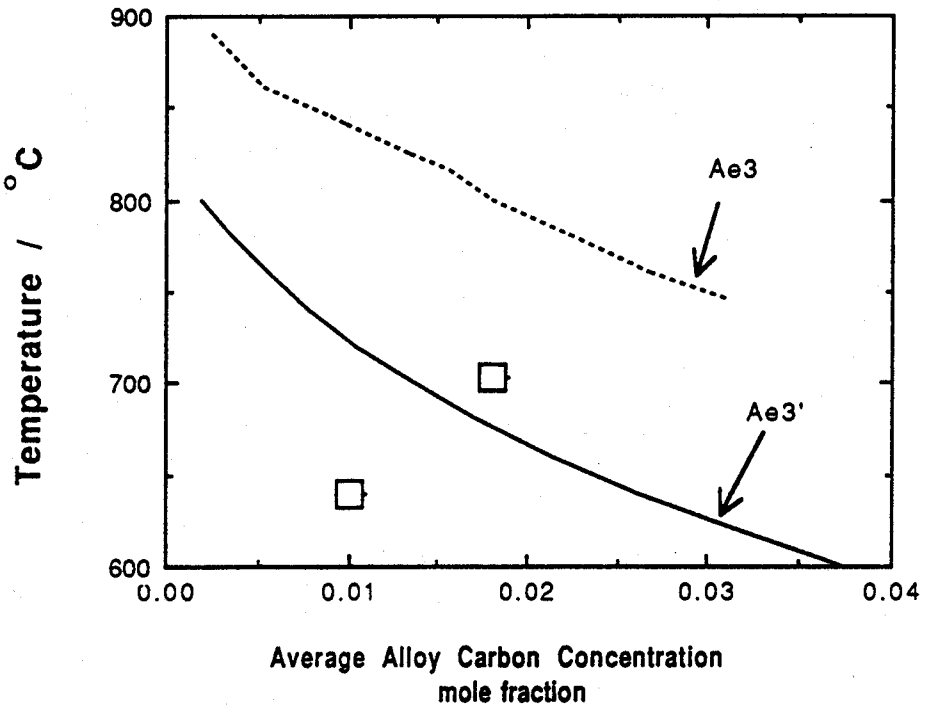


Fig. 7.12 Plot of calculated Ae3 and Ae3' phase boundaries for various average alloy carbon concentration for a Fe-2Si-3Mn (wt.%) alloy system (MTDATA, 1989, Bhadeshia and Edmonds, 1980). The square symbols indicate the composition of alloys A1 and A2 and temperature at which they were heat treated to form allotriomorphic ferrite.